Preface

This work has been carried out during the years 1999-2006 at the Department of Physics in the University of Jyväskylä.

I wish to thank my supervisor Prof. Jouni Suhonen for competent and motivating guidance and for introducing me to the field of theoretical nuclear physics. I am also grateful to Prof. (emeritus) Pertti Lipas, Dr. Matias Aunola and Dr. Teemu Siiskonen for help and guidance.

It has been pleasure to work at the Department of Physics. Warmest thanks goes to the whole staff at the department for creating pleasant and open atmosphere.

I would like to thank all my friends for their friendship and support.

The financial support from the Academy of Finland under the Finnish Centre of Excellence Programme 2000–2005 (Project No. 44875, Nuclear and Condensed Matter Programme at JYFL) and the Finnish Centre of Excellence Programme 2006–2011 (Nuclear and Accelerator Based Program at JYFL) is gratefully acknowledged.

Finally, I want to thank my parents for their love and support.

Jyväskylä, April 2006

Markus Kortelainen

ISBN 978-951-39-3167-4

URN:ISBN:978-951-39-3167-4

Abstract

The ordinary muon capture (OMC) is suggested to be used as a probing tool in order to gain information about the structure of the intermediate nuclear states involved in the double beta ($\beta\beta$) decay. It has been demonstrated that the nuclear-structure aspects in the $\beta\beta$-decay calculations can be fine tuned by the information gained from the measurements of the partial OMC rates from the ground state of the initial or final nucleus to the intermediate states within a $\beta\beta$ decay chain. It has been found that the calculated OMC observables as well as the two-neutrino double beta ($2\nu\beta\beta$) amplitudes depend strongly on the involved nuclear structure.

In nuclear-structure calculations both the nuclear shell model (SM) and the proton-neutron quasiparticle random-phase approximation (pnQRPA) have been employed. For the light nuclei the SM calculations indicate that the states with biggest OMC rates are also the most relevant ones in the $2\nu\beta\beta$ decay. The effect of the mean field on the OMC rates is also studied. The structure of heavier nuclei was calculated by using the pnQRPA. The pnQRPA calculations involve the particle-particle interactions strength parameter $g_{\rm pp}$. It was found that $g_{\rm pp}$ affects strongly the calculated OMC rates. The role of the induced pseudoscalar current and its coupling constant $g_{\rm P}$ in the OMC is also discussed.

List of publications

This thesis is a review of the following publications:

I **Mean-field effects on muon-capture observables**
M. Kortelainen, M. Aunola, T. Siiskonen and J. Suhonen,
J. Phys G: Nucl. Part. Phys 26 (2000) 33.

II **Ordinary muon capture as a probe of virtual transitions of $\beta\beta$ decay**
M. Kortelainen and J. Suhonen,
Eur. Phys. Lett, 58 (2002) 666.

III **Microscopic study of muon-capture transitions in nuclei involved in double-beta-decay processes**
M. Kortelainen and J. Suhonen,
Nucl. Phys. A, 713 (2003) 501.

IV **Analysis of the $2\nu\beta\beta$ decay and muon-capture reactions for the mass $A = 46$ and $A = 48$ nuclei using the nuclear shell model**
M. Kortelainen and J. Suhonen,
Phys. At. Nucl. 67 (2004) 1202.

V **Nuclear muon capture as a powerful probe of double beta decays in light nuclei**
M. Kortelainen and J. Suhonen,
J. Phys. G: Nucl. Part. Phys. 30 (2004) 2003.

VI **Probing double beta decay by the nuclear muon capture**
M. Kortelainen and J. Suhonen,
Muons: New Research, Nova Science Publishers Inc., New York (2005).

The author of this thesis has written papers III-VI. The author has made the nuclear structure calculations of IV and V, and all the other calculations for all papers. The author has developed the code used in the OMC calculations and written the code for $2\nu\beta\beta$ decays. Publication VI is an invitated article with some new results.

Contents

1 Introduction

The atomic nucleus is a many-body system where three of the four fundamental interactions play an important role. This feature makes the nucleus an interesting and challenging subject of study. The two strongest interactions – nuclear and electromagnetic – are responsible for nuclear structure, while the effect of the weak interaction can be seen in radioactive decays of nuclei. The fourth interaction, gravitation, is known to play a negligible role in the physics of the nucleus. The theories of the weak and electromagnetic interactions can be unified to yield one single theory: the theory of electro-weak interaction. This, together with the theory of strong interactions, forms the standard model of particle physics. Currently, attempts are being made to unify the theories of all the four interactions to one single theory.

A typical way to study the atomic nuclei experimentally is to analyze nuclear reactions. These can be, for example, radioactive decays or scatterings of two nuclei off each other in collision processes. In these experiments the initial state of the system is either known or prepared in some specific way and the final state can be measured. The measured observables yield information on the nuclear process under study. Based on this information one can construct theoretical models about the structure of the nucleus and the interactions between its constituents, the nucleons.

The purpose of the present work is to study nuclear structure and nuclear decay by using one particular type of a weak-interaction process, namely the nuclear muon capture. The muon capture can happen in a muonic atom where, in addition to the electrons, a muon orbits the nucleus. As a result it is possible that the orbiting muon is captured by one of the protons of the nucleus. By comparing the calculated results for the muon-capture rates to the corresponding experimental ones, one can gain information about the involved nuclear wave functions. Furthermore, the present work demonstrates how this information can be exploited in the calculations of a second-order weak-interaction process known as the nuclear double beta decay.

The double beta decay is a very rare process and for this reason the experimental set-ups are located deep under ground in order to minimise the background radiation. The focus of the present-day experimental set-ups is on detection of the neutrinoless double beta decay, since it has a lot of relevance in search for new physics beyond the standard model. This search is an active topic in physics due to the fact that there is clear experimental evidence about the existence of a non-zero neutrino mass which is non-existent in the framework of the standard model.

2 Nuclear structure

Explaining nuclear structure is a challenging theoretical problem. Due to its many-body nature the structure of a given nucleus can not be solved exactly. On the other hand, there are too few nucleons in nuclei to allow for a statistical treatment of the problem. Therefore, one has to make approximations. The usual starting point is the nuclear mean-field approximation, where every nucleon is assumed to move in a potential created by all the other nucleons in a nucleus. In this approximation the nuclear Hamiltonian

$$H = \sum_{\alpha\beta} t_{\alpha\beta} c_\alpha^\dagger c_\beta + \frac{1}{4} \sum_{\alpha\beta\gamma\delta} \bar{v}_{\alpha\beta\gamma\delta} c_\alpha^\dagger c_\beta^\dagger c_\gamma c_\delta \,, \tag{1}$$

where $t_{\alpha\beta}$ is the single-particle energy term and $\bar{v}_{\alpha\beta\gamma\delta}$ the antisymmetrised two-particle interaction term, can be written as

$$H = \sum_{\alpha\beta} \left(t_{\alpha\beta} c_\alpha^\dagger c_\beta + \frac{1}{4} v_{\alpha\beta} c_\alpha^\dagger c_\beta \right) + \frac{1}{4} \sum_{\alpha\beta\gamma\delta} \left(\bar{v}_{\alpha\beta\gamma\delta} c_\alpha^\dagger c_\beta^\dagger c_\gamma c_\delta - v_{\alpha\beta} c_\alpha^\dagger c_\beta \right) . \tag{2}$$

Above $v_{\alpha\beta}$ denotes the mean field potential. In this way the nuclear Hamiltonian (2) has been divided into two parts

$$H = H_{\mathrm{MF}} + V_{\mathrm{RES}} \,, \tag{3}$$

where

$$H_{\mathrm{MF}} = \sum_{\alpha\beta} \left(t_{\alpha\beta} c_\alpha^\dagger c_\beta + \frac{1}{4} v_{\alpha\beta} c_\alpha^\dagger c_\beta \right) \tag{4}$$

is the mean field Hamiltonian and

$$V_{\mathrm{RES}} = \frac{1}{4} \sum_{\alpha\beta\gamma\delta} \left(\bar{v}_{\alpha\beta\gamma\delta} c_\alpha^\dagger c_\beta^\dagger c_\gamma c_\delta - v_{\alpha\beta} c_\alpha^\dagger c_\beta \right) \tag{5}$$

is the residual interaction. Thus, the mean field part (4) allows to treat, to first approximation, the strongly interacting many-fermion system as a group of non-interacting fermions moving in a central potential $t_{\alpha\beta} + 1/4 v_{\alpha\beta}$. By solving the Schrödinger equation for the Hamiltonian H_{MF} one gets the single-particle basis, i.e. the orbitals where the nucleons move independently in the mean-field approximation. The labeling of these mean-field orbitals follows the convention $\alpha = a, m_\alpha = n_a, l_a, j_a, m_\alpha$.

The magnitude of the residual interaction V_{RES} is typically a lot smaller than the magnitude of the mean-field Hamiltonian H_{MF}. This allows for a perturbative treatment of the total nuclear Hamiltonian H, where H_{MF} is considered to be the unperturbated Hamiltonian and V_{RES} a small perturbation. To obtain the optimal H_{MF} one has to minimize the residual interaction V_{RES}, which leads to a self-consistent

mean field. However, for simplicity, it is common to take the mean-field potential to be a harmonic oscillator or Woods-Saxon potential.

There are ways to obtain the residual interaction $V_{\rm RES}$ in a self-consistent manner, e.g. by the Hartree-Fock scheme. There are also attempts to mimic it in approximative, empirical ways. One example of the latter is the simple schematic surface-delta interaction, which gives reasonable results for nuclear observables in many cases. One can also treat all the single-particle energies and two-body interaction matrix elements as fitting parameters in order to reproduce certain experimental data. The USD interaction [1] is a typical example of a fitted interaction. There are also interactions which are derived from a meson-exchange picture of the nuclear force, like for example the Bonn one-boson-exchange potential [2].

In order to reproduce the so-called magic numbers observed in the shell structure of nuclei, it was found by Goeppert-Mayer [3] that one needs to add a strong spin-orbit term to the nuclear Hamiltonian. This, together with the central mean-field potential, leads to a grouping of the single-particle levels to "shells". These shells contain from one to several single-particle orbitals with small energy differences in the single-particle energies as compared to the energy width of the adjacent shell gaps. Due to this tendency to form separate energy shells, the nuclear-structure calculations can be simplified considerably. On many occasions it is enough to consider only those nucleons, which occupy the valence shell(s). The completely filled shells, below the active valence shells, can be treated as an inert core, not participating in the nuclear-structure calculations.

2.1 The nuclear shell model

At the mean-field level valence nucleons are distributed to the single-particle orbitals to form various possible configurations. Each configuration has its associated configuration energy which is the sum of the single-particle energies of the occupied orbitals. The ground-state configuration, where all the single-particle orbitals are occupied up to the proton and neutron Fermi energies, has the lowest configuration energy. The residual interaction mixes all the possible configurations thus producing the various nuclear states. Calculation of the effects of this many-nucleon configuration mixing is the task of the nuclear shell model. Numerics of this task are treated by using various types of shell-model computer codes.

Shell-model codes mainly work either in the m-scheme or j-scheme. In addition, there are also Monte-Carlo shell-model codes, which are not discussed here. The m-scheme states have definite value for the z-component of the total angular momentum, but they are not states of good angular momentum. However, the eigenstates obtained from the diagonalization of the Hamiltonian matrix do have the symmetries of the nuclear Hamiltonian.

The j-scheme states are angular-momentum projections of the m-scheme states. The advantage of the j-scheme is the reduction of the Hamiltonian matrix to a block-

diagonal form. Each block has its own definite angular momentum and can be diagonalized separately. The disadvantage of the j-scheme lies in the projection of the j-scheme states, which is time consuming and sensitive to numerical rounding errors. The shell-model code OXBASH [4], which was used in our calculations, works in a mixed scheme. The Hamiltonian matrix is diagonalised in the j-scheme, but the resulting eigenvectors are written in the m-scheme basis.

The calculation of the matrix element for a given one-body operator $\mathcal{O}_\lambda$ can be done in the occupation-number representation. In this way the matrix element can be expressed as a sum of single-particle transitions, weighted with terms coming from the many-particle nuclear structure, i.e.

$$(J_\mathrm{f}||\mathcal{O}_\lambda||J_\mathrm{i}) = \hat{\lambda}^{-1} \sum_{ab} (a||\mathcal{O}_\lambda||b)(J_\mathrm{f}||\left[c_a^\dagger \tilde{c}_b\right]_\lambda||J_\mathrm{i})\,. \tag{6}$$

The term $(J_\mathrm{f}||\left[c_a^\dagger \tilde{c}_b\right]_\lambda||J_\mathrm{i})$ above represents the many-particle nuclear structure and is called one-body transition density. This part can be calculated by the shell-model codes.

The drawback of the shell model is the fact that the number of possible configurations increases combinatorially as the number of available single-particle orbitals and the number of valence nucleons increases. This leads quite rapidly to huge memory and CPU-time requirements. For this reason realistic shell-model calculations can not be applied to most of the medium-heavy and heavy nuclei. Therefore, one has to apply other methods for nuclear-structure calculations of these nuclei. One popular alternative for the shell model is the quasiparticle random-phase approximation (QRPA) and its variants.

2.2 The BCS and pnQRPA

Due to the strong pairing interaction in nuclei, all of the nuclei with even number of protons and even number of neutrons have their ground-state spin and parity 0^+. Pairing is also present in the electron theory of superconductivity by Bardeen, Cooper and Schrieffer (BCS) and this theory can be applied to many-nucleon systems with some modifications. Thus, the ground state of an even-even nucleus can be treated as a superconducting state where all the protons and neutrons have been paired to form zero-angular-momentum Cooper pairs.

The BCS ground state $|\mathrm{BCS}\rangle$ is a linear combination of states with different numbers of nucleons. It can be written in the form

$$|\mathrm{BCS}\rangle = \prod_{a,m_\alpha>0} \left(u_a - v_a c_{a,m_\alpha}^\dagger \tilde{c}_{a,m_\alpha}^\dagger\right)|\mathrm{CORE}\rangle\,, \tag{7}$$

where the coefficients v_a and u_a represent occupation and unoccupation numbers of a state a. Furthermore, $|\mathrm{CORE}\rangle$ represents the inert core of the discussed nucleus and it can be treated as an effective particle vacuum, i.e. $c_\alpha|\mathrm{CORE}\rangle = 0$.

The BCS quasiparticle creation and annihilation operators can be derived by using the Bogoliubov-Valatin transformation. In this transformation the quasiparticle annihilation operator becomes

$$a_\alpha = u_a c_\alpha + v_a \tilde{c}^\dagger_\alpha \,, \tag{8}$$

and it annihilates, as it should, the BCS quasiparticle vacuum i.e. $a_\alpha|\mathrm{BCS}\rangle = 0$. The corresponding quasiparticle creation operator is by Hermitean conjugation

$$a^\dagger_\alpha = u_a c^\dagger_\alpha + v_a \tilde{c}_\alpha \,. \tag{9}$$

The requirement to satisfy the fermion anticommutation relation $\{a^\dagger_\alpha, a_\beta\} = \delta_{\alpha\beta}$ leads to the condition

$$u_a^2 + v_a^2 = 1 \,. \tag{10}$$

Condition (10) can also be viewed as a probability normalization thus leading to the interpretation of v_a and u_a as occupation and unoccupation amplitudes.

The nuclear Hamiltonian of Eq. (1) can be written by using the quasiparticle operators. In this way the Hamiltonian can be cast in a form

$$\hat{H} = H_{11} + H_{02} + H_{20} + H_{22} + H_{04} + H_{13} + H_{31} + H_{40} \,, \tag{11}$$

where each term H_{nm} is proportional to the product $a^\dagger_{\alpha_1} a^\dagger_{\alpha_2} \cdots a^\dagger_{\alpha_n} a_{\beta_1} a_{\beta_2} \cdots a_{\beta_m}$. Here the terms H_{11}, H_{02} and H_{20} can be associated to a quasiparticle mean field with quasiparticle energies E_a. The rest of the terms represent residual interactions among the quasiparticles. Numerical values of the occupation and unoccupation amplitudes v_a and u_a and the quasiparticle energies E_a can be calculated by using a variational procedure. The variation is performed separately for protons and neutrons.

As mentioned, the BCS vacuum describes the ground state of an even-even nucleus. In order to describe the excited states, or states of an odd-odd nucleus, one needs to build two-quasiparticle excitations. The proton-neutron QRPA (pnQRPA) theory, introduced by Hableib and Sorensen [5], describes the states of an odd-odd nucleus as proton-neutron quasiparticle excitations built atop of the QRPA vacuum. These proton-neutron quasiparticle excitations, coupled to good angular momentum J and its z-projection M, can be written as [6, 7]

$$A^\dagger(pn, JM) = \left[a^\dagger_p a^\dagger_n\right]_{JM} ; \quad \tilde{A}(pn, JM) = (-1)^{J+M} \left(A^\dagger(pn, JM)\right)^\dagger \,. \tag{12}$$

The one-phonon ansatz of the pnQRPA can be written by using the above defined two-quasiparticle operators and it has the form

$$Q^\dagger_{JM}(m) = \sum_{pn} \left[X_{pn}(J^\pi, m) A^\dagger(pn, JM) - Y_{pn}(J^\pi, m) \tilde{A}(pn, JM)\right] \,, \tag{13}$$

where X_{pn} (Y_{pn}) is the so called forward- (backward-) going amplitude. Magnitudes of the backward-going amplitudes Y_{pn} are a good measure of the amount of the pnQRPA ground-state correlations.

The pnQRPA equations of motion have the general form

$$\begin{pmatrix} A & B \\ B & A \end{pmatrix} \begin{pmatrix} X \\ Y \end{pmatrix} = \Omega \begin{pmatrix} 1 & 0 \\ 0 & -1 \end{pmatrix} \begin{pmatrix} X \\ Y \end{pmatrix} . \tag{14}$$

The states of the double-odd nucleus can be obtained by solving the non-Hermitian eigenvalue problem described by Eq. (14). The sub-matrices A and B of Eq. (14) are defined as follows

$$\begin{aligned} A_{pnp'n'} &= \delta_{pp'}\delta_{nn'}(E_p + E_n) - 2g_{\rm pp}G(pnp'n', J)(u_p u_n u_{p'} u_{n'} + v_p v_n v_{p'} v_{n'}) \\ &\quad -2g_{\rm ph}F(pnp'n', J)(u_p u_n v_{p'} v_{n'} + v_p v_n u_{p'} u_{n'}) \qquad (15) \\ B_{pnp'n'} &= 2g_{\rm pp}G(pnp'n', J)(u_p u_n v_{p'} v_{n'} + v_p v_n u_{p'} u_{n'}) \\ &\quad -2g_{\rm ph}F(pnp'n', J)(u_p v_n v_{p'} u_{n'} + v_p u_n u_{p'} v_{n'}) , \qquad (16) \end{aligned}$$

where E_p and E_n are the proton and neutron quasiparticle energies. Furthermore, $G(pnp'n', J)$ and $F(pnp'n', J)$ are the two-body particle-particle and particle-hole interaction matrix elements defined by Baranger [8].

The coefficients $g_{\rm pp}$ and $g_{\rm ph}$ are scaling factors for the particle-particle and particle-hole interaction strengths. The parameter $g_{\rm ph}$ is usually adjusted by the empirical data on the energy of the Gamow-Teller giant resonance excitation. The coefficient $g_{\rm pp}$, however, is often left as a free parameter of the theory. As a matter of fact, the sub-matrix A in Eq. (14) is the pnQTDA matrix, which appears in a more simple theory called the proton-neutron quasiparticle Tamm-Dancoff approximation. The pnQTDA theory does not take into account the correlations of the ground state.

The β^- and β^+ type of decay amplitudes between a J^π pnQRPA one-phonon state and the pnQRPA ground state can be expressed as [7]

$$(J^\pi, m||M^-_\lambda||{\rm QRPA}) = \delta_{J\lambda} \sum_{pn} (p||M_\lambda||n) \left[u_p v_n X_{pn}(J^\pi, m) + v_p u_n Y_{pn}(J^\pi, m)\right] , \tag{17}$$

$$(J^\pi, m||M^+_\lambda||{\rm QRPA}) = -\delta_{J\lambda} \sum_{pn} (p||M_\lambda||n) \left[u_n v_p X_{pn}(J^\pi, m) + v_n u_p Y_{pn}(J^\pi, m)\right]. \tag{18}$$

3 Weak interaction

In the first beta-decay experiments it was found that the outgoing electron has a continuous energy distribution instead of a fixed value of energy. This seemed to go against the conservation of energy. Moreover, beta decay also seemed to violate the conservation of angular momentum. In order to conserve these quantities Wolfgang Pauli suggested that there should be also another particle emitted in the beta decay – the neutrino. The neutrino was assumed to be neutral, massless and weakly interacting. This lead Enrico Fermi to formulate his theory of beta decay [9].

The Fermi theory of beta decay was applied broadly to many phenomena. Besides the beta decay of atomic nuclei, it was used to describe phenomena such as the decay of a muon and several other particles, muon capture of the atomic nucleus, etc. However, the drawback of the Fermi theory lies in the fact that it assumes the interaction to be point-like. This leads to ultraviolet divergences and therefore Fermi theory is not renormalizable.

The picture of the weak interaction got more accurate by the introduction of the electro-weak interaction of the standard model [10]. In the standard model there are three generations of leptons and quarks and, thus, three differed kinds of neutrino. The neutrinos of the standard model are assumed to be massless Dirac particles, i.e. the antineutrino is not the same particle as the neutrino. Furthermore, the standard model also assumes lepton-number conservation for each generation separately.

Recent neutrino-oscillation experiments [11, 12, 13, 14] have revealed that the standard model's picture of the neutrinos is not sufficient. In these experiments it has been observed that the flavour of a neutrino can change due to flavour oscillation. Moreover, the flavour oscillation requires neutrino to have mass. Unfortunately, the neutrino-oscillation experiments cannot access the absolute mass scale of the neutrino, only the mass differences between the neutrino mass eigenstates. At the preset only upper limits of the neutrino mass have been determined. The determination has been done by cosmological observations [15] or by kinematical analysis of the electron spectrum in beta decay [16]. In addition to the unknown mass of the neutrino, the question of neutrino being either a Dirac or Majorana type of particle is still open. However, the neutrinoless double beta decay can answer both of these questions.

The double beta decay is one of the slowest processes in nature. It can occur in nuclei with even numbers of protons and neutrons. Due to the nuclear short-range pairing forces, the binding energy of a double-odd nucleus may be smaller than the binding energy of its double-even isobaric neighbour nuclei. In this kind of situation it is possible that the ordinary beta decay of some double-even nuclei, not located at the bottom of the valley of beta stability, is energetically forbidden. In some cases the ordinary beta decay is energetically possible but highly forbidden due to the large difference in angular momentum between the mother and daughter states. Nevertheless, in this kind of situation the nuclear double beta decay allows a double-even nucleus to decay directly to states of lower energy in the neighbouring

double-even isobaric nucleus. This is illustrated in Fig. 1, where the isobars $A = 136$ have been chosen as examples. As can be seen, ^{136}Xe cannot decay via ordinary beta decay. The situation is also the same for ^{136}Ce. However, both of these nuclei can disintegrate via the double beta decay.

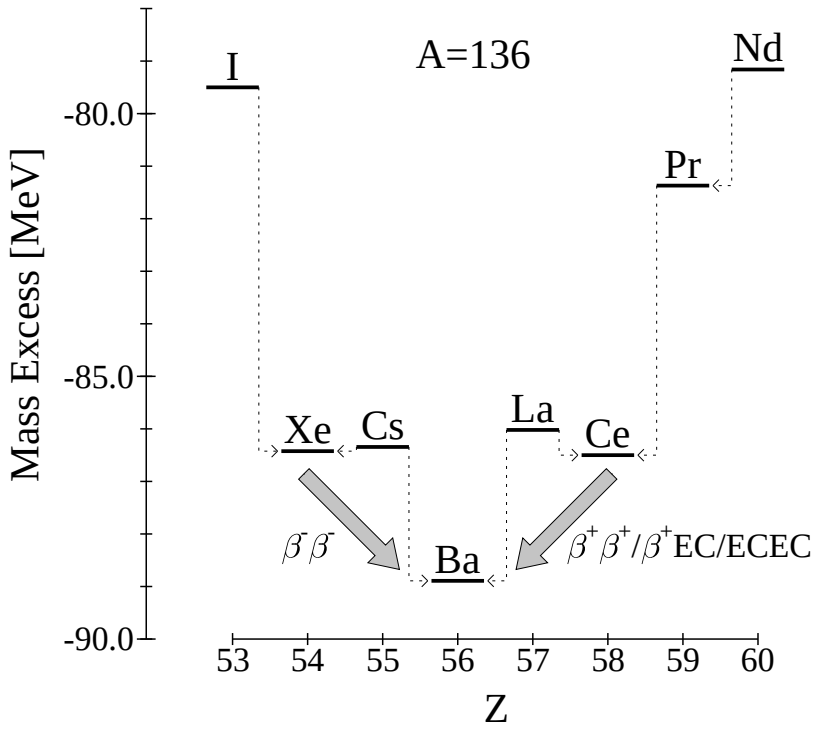

Figure 1: Mass excess of the $A = 136$ isobars as a function of the proton number Z. The dashed arrows represent beta decays and the thick arrows represent double beta decays.

There exist two different modes of double beta decay. The first mode, two-neutrino double beta ($2\nu\beta\beta$) decay, conserves the lepton number and, therefore, is allowed in the standard model's framework. Thus, as the name indicates, the final state of the $2\nu\beta\beta$ decay contains two neutrinos. The $2\nu\beta\beta$ decay was first predicted by Maria Goeppert-Mayer in 1935 [17]. The $2\nu\beta\beta$ decay has been experimentally observed in several nuclei, and the shortest observed half-lives are of the order of 10^{19} y [18].

In contrast to the $2\nu\beta\beta$ decay, the neutrinoless double beta ($0\nu\beta\beta$) decay violates the conservation laws of the standard model. As the name indicates, there are no neutrinos in the final state and therefore the lepton-number conservation is violated by $\Delta L = 2$. The existence of the $0\nu\beta\beta$ decay was first proposed by Furry in 1939 [19]. The $0\nu\beta\beta$ decay allows the access to the mass scale of the neutrino. This is due to the fact that the inverse of the $0\nu\beta\beta$ half-life is proportional to the second power of the effective

mass $\langle m_\nu \rangle$ of the neutrino. Moreover, according to the Schechter-Valle theorem [20], the existence of the $0\nu\beta\beta$ decay implies that the neutrino is a Majorana particle with non-zero mass. To extract the effective neutrino mass from the experiments, one needs information about the involved nuclear matrix elements [7]. The absolute neutrino mass can be obtained from the effective mass by using the available information about the neutrino mixing [21] and CP phases. There even exists a claim that the $0\nu\beta\beta$ decay has been observed in ^{76}Ge with a half-life of $T_{1/2} = (1.19^{+0.37}_{-0.23}) \times 10^{25}$ y [22], leading to an effective neutrino mass of $\langle m_\nu \rangle = 0.2 - 0.6$ eV. This result is, however, under debate [23, 24]. The next-generation double-beta-decay experiments will probably shed light on this issue.

The first attempts for nuclear-structure calculations of double-beta-decay rates mostly concentrate on using the nuclear shell model as a starting point. Unfortunately, due to the fact that the $\beta\beta$-decaying nuclei are medium-heavy or heavy nuclei, severe truncations of the configuration space, or the use of the weak coupling limit, are needed. For this reason, other methods have been used, the pnQRPA and its variants being the most popular ones. However, as mentioned earlier in section 2.2 the disadvantage of the pnQRPA theory lies in the somewhat uncertain value of the particle-particle interaction strength parameter $g_{\rm pp}$. The parameter $g_{\rm pp}$ has strong influence on theoretical predictions of the nuclear structure and, therefore, on the calculated half-lives of the $\beta\beta$-decay.

In the theoretical description of the double beta decay the transitions proceed via the states of the intermediate nucleus. In the case of the $2\nu\beta\beta$ decay only the 1^+ states of the intermediate nucleus are active, whereas in the case of the $0\nu\beta\beta$ decay, all the J^π states of the intermediate nucleus are active. A reliable theoretical description of the structure of these states is essential in theoretical calculations. As mentioned, the $g_{\rm pp}$ parameter plays a crucial role in the $\beta\beta$-decay rate calculations.

In some works [7, 25] the values of the $g_{\rm pp}$ parameter of the $\beta\beta$-decay calculations have been adjusted by using the available data on the beta-decay or electron-capture transitions. These transitions run from the intermediate nucleus to the final or initial state of the corresponding $\beta\beta$ decay. Unfortunately, this information is usually available only for one state, typically the ground state of the intermediate nucleus. Recently, it has been suggested to use the experimental data on the $2\nu\beta\beta$ decay half-lives to obtain the nuclear matrix elements involved in the corresponding $0\nu\beta\beta$ decays [26]. However, there are some pitfalls in this method, as pointed out in [27]. It has also been proposed that one could use charged-current neutrino-nucleus interactions as a probe of the virtual transitions involved in the $0\nu\beta\beta$ decay [28]. Unfortunately, due to the extremely small cross section of the neutrino-nucleus charged-current reaction, the experimental setup would require neutrino-beam intensities which cannot be achieved at the present.

One method to study the structure of the states of the intermediate nucleus of double beta decay is to perform muon-capture experiments. The ordinary muon capture (OMC) process allows to study one leg of the virtual transitions involved in

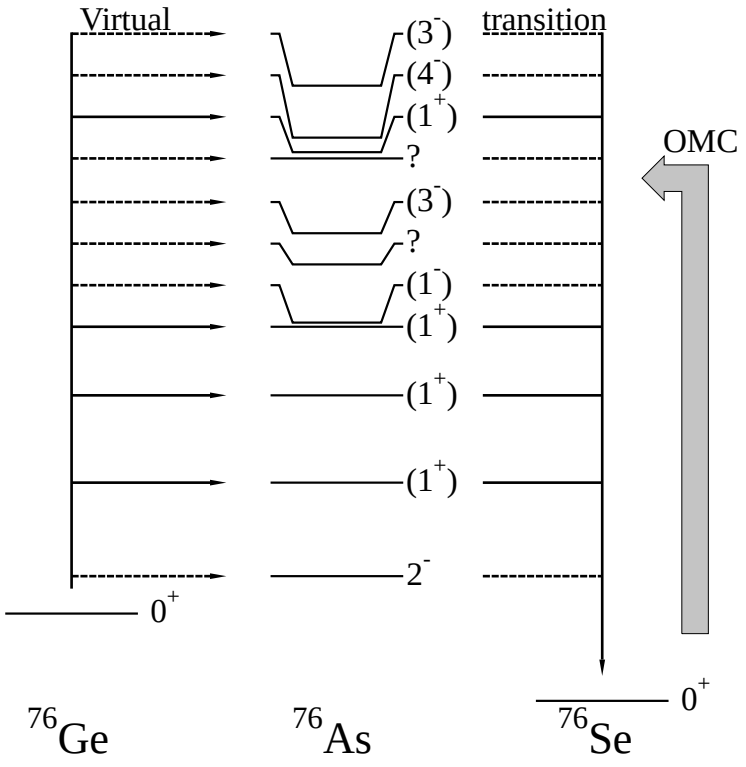

Figure 2: A schematic illustration of the connection between the $\beta\beta$-decay and ordinary muon capture. In the $2\nu\beta\beta$ decay the transition proceeds via the 1^+ states of the intermediate nucleus (solid lines), whereas in the $0\nu\beta\beta$ decay all the intermediate states are active (solid and dashed lines).

double beta decays. This is demonstrated in Fig. 2, where the $\beta\beta$ decay of ^{76}Ge has been taken as an example. By measuring the OMC rates in transitions from the ground state of ^{76}Se to the states of ^{76}As one could gain information about the structure of these states. In spite of the fact that the OMC probes only one of the two branches involved in double beta decay, it can provide a lot of valuable information which can be used in $\beta\beta$-decay calculations. Due to the large mass of the muon, about 100 MeV, the final state of the OMC can be highly excited. Therefore, in principle, it is possible to study all the relevant intermediate states of double beta decay. Moreover, another consequence of the large mass of the muon is the fact that forbidden transitions are not as suppressed as in the case of the electron capture or beta decay. As a matter of fact, transition rates to some of the 2^- states can even be higher than transition rates to 1^+ states. This allows to study also intermediate states with spin and parity other than 1^+. These states are potentially relevant in the $0\nu\beta\beta$ decay [29].

3.1 Ordinary muon capture

When a negative muon is stopped in matter, in the outer shells of atoms, it undergoes several electromagnetic transitions to lower atomic orbitals, accompanied by emission of muonic X-rays. Energies of these X-rays can reach up to an order of MeV in heavier nuclei. Finally, the muon ends up into the K atomic orbit. As a result, it is possible that the muon is captured by a nucleus in a process $\mu^- + (A, Z) \rightarrow \nu_\mu + (A, Z-1)^{(*)}$, where the asterisk denotes the possibility that the final nuclear state can be an excited state. The OMC competes with the decay of the muon. In addition to the OMC there exist also other processes in muonic atoms. In the radiative muon capture the final state also contains a gamma-ray. Also, in the case of some heavy nuclei the muon capture can lead to fission of the final nucleus.

There exists a phenomenological estimate by Primakoff to the total muon capture rate $W_{\rm tot}$:

$$W_{\rm tot} = Z_{\rm eff}^4 X_1 \left[1 - X_2 \left(\frac{A-Z}{2A} \right) \right] , \tag{19}$$

where $Z_{\rm eff}$ is the effective charge of the nucleus [30]. Furthermore, the coefficients X_n can be fitted to the experimental data giving the values $X_1 = 170\ {\rm s}^{-1}$ and $X_2 = 3.125$. However, this approach is not fruitful from the nuclear-structure point of view since we need information on capture to individual nuclear states. In [31] the authors calculated the total muon capture rates in the RPA basis and obtained results similar to the ones coming from eq. (19). According to their calculations the RPA formalism reproduces total OMC rates quite reliably.

The formalism needed for the calculation of the OMC rate was developed by Morita and Fujii in Ref. [32]. In their work they started from the most general Hamiltonian density

$$H = \bar{\psi}_{\rm n} \mathcal{H} \psi_{\rm p} \, , \tag{20}$$

with

$$\begin{aligned} \sqrt{2}\mathcal{H} \;=\; & \gamma^\lambda C_V \left[\bar{\psi}_\nu \gamma_\lambda \psi_\mu + \bar{\psi}_\nu \gamma_\lambda \gamma^5 \psi_\mu \right] \\ & - \gamma^\lambda \gamma^5 C_A \left[\bar{\psi}_\nu \gamma_\lambda \psi_\mu + \bar{\psi}_\nu \gamma_\lambda \gamma^5 \psi_\mu \right] \\ & + \gamma^5 C_P \left[\bar{\psi}_\nu \gamma^5 \psi_\mu - \bar{\psi}_\nu \psi_\mu \right] \\ & + \sigma^{\lambda\rho} C_M \left[p_\rho (\bar{\psi}_\nu i \gamma_\lambda \psi_\mu) + p_\rho (\bar{\psi}_\nu i \gamma_\lambda \gamma^5 \psi_\mu) \right] , \end{aligned} \tag{21}$$

where $\sigma^{\lambda\rho} = \frac{1}{2} \left[\gamma^\lambda \gamma^\rho - \gamma^\rho \gamma^\lambda \right]$ and $p_\rho = (i\partial/\partial t \, , \, i\nabla)$. However, due to the fact that the weak magnetism coupling constant is proportional to the vector coupling constant, $C_M = C_V [\mu_{\rm p} - \mu_{\rm n}]/2M \approx 3.706 C_V/2M$, there are actually only three independent coupling constants, namely C_V, C_A, and C_P.

In the shell-model calculations of beta-decay rates the coupling constants C_V and C_A are also present. In these calculations a typical value adopted for the ratio of the vector coupling constant and the axial-vector coupling constant is $C_A/C_V = -1.0$,

instead of the bare nucleon value $C_A/C_V \approx -1.25$ [33, 34]. In the present work the ratio $C_A/C_V = -1.0$ has been used for the OMC calculations.

The value of the pseudoscalar coupling constant is fixed by the partially conserved axial-vector current (PCAC) hypothesis, giving rise to a nuclear-model independent estimate $C_P/C_A \approx 7$ (see e.g. [35]). However, the value of the pseudoscalar coupling constant may need to be renormalized in the nuclear medium, like in the case of the axial-vector coupling constant.

The transition rate for the OMC can be derived from the Hamiltonian density of Eq. (20) [32]. The derivation is done by making the standard non-relativistic reduction of the nucleon operators. The lepton part is kept relativistic and the small component of the muon bound state wave function has been set to zero. This approximation is valid since in our calculated cases $(\alpha Z)^2 \ll 1$, where α is the fine-structure constant. The effect of the small component is of the order of a few percent [36].

By performing a summation over all magnetic quantum numbers and integrating over the neutrino momentum one ends up with following expression for the transition rate

$$W = 4P(\alpha Z m'_\mu)^3 \frac{2J_\mathrm{f}+1}{2J_\mathrm{i}+1}\left(1 - \frac{q}{m_\mu + AM}\right) q^2, \tag{22}$$

with

$$q = (m_\mu - W_0)\left(1 - \frac{m_\mu - W_0}{2(M_\mathrm{F} + m_\mu)}\right) \tag{23}$$

and A being the mass number of the initial and final nuclei, Z the charge number of the initial nucleus, and m'_μ the reduced muon mass. Furthermore, M denotes the average nucleon mass and $W_0 = M_\mathrm{F} - M_\mathrm{I} + m_\mathrm{e} + E_\mathrm{x}$, with M_F and M_I denoting the final and initial atomic masses. The quantity P in Eq. (22) contains all the nuclear-physics aspects of the reaction, in particular it contains the reduced nuclear matrix elements $\mathcal{M}[kwu]$. Definition of the term P can be found e.g. in Refs. [32, V]. The term $(\alpha Z m'_\mu)^3$ in eq. (22) comes from the amplitude of the muon wave function at the origin in the nonrelativistic case. The effect of the relativistic corrections in this term are of the order of few per cent or less in our calculated cases, as deduced from the expressions of [32]. The reduced matrix elements are defined as follows

$$\begin{aligned}&\int U_{J_\mathrm{f}M_\mathrm{f}} \sum_{s=1}^{A} e^{-\alpha Z m'_\mu r_s} \Psi_s \tau_-^s U_{J_\mathrm{i}M_\mathrm{i}} dr_1 \ldots dr_A \\ &= \mathcal{M}[kwu\binom{\pm}{p}](J_\mathrm{i}\, M_\mathrm{i}\, u\, M_\mathrm{f} - M_\mathrm{i} | J_\mathrm{f}\, M_\mathrm{f})\ ,\end{aligned} \tag{24}$$

where $U_{J_\mathrm{f}M_\mathrm{f}}$ and $U_{J_\mathrm{i}M_\mathrm{i}}$ are the final and initial nuclear wave functions, respectively. The factor Ψ_s is defined in Table 1. The quantity $\mathcal{Y}^M_{kwu}$ in Table 1 is the vector

spherical harmonic and it is defined as

$$\mathcal{Y}^M_{0wu} \equiv (4\pi)^{-1/2} Y^M_w(\hat{\mathbf{r}}) \,, \tag{25}$$

$$\mathcal{Y}^M_{1wu} \equiv \sum_m (1\ -m\, w\, m+M|u\, M) Y^{m+M}_w(\hat{\mathbf{r}}) \sqrt{\frac{3}{4\pi}} \sigma_{-m} \,. \tag{26}$$

Table 1: Definition of the reduced matrix elements for the muon capture.

Matrix element	Ψ_s
$\mathcal{M}[0wu]$	$j_w(qr_s)\mathcal{Y}^{M_f-M_i}_{0wu}(\hat{r}_s)\delta_{wu}$
$\mathcal{M}[1wu]$	$j_w(qr_s)\mathcal{Y}^{M_f-M_i}_{1wu}(\hat{r}_s,\sigma_s)$
$\mathcal{M}[0wu\pm]$	$\Big[j_w(qr_s)\pm\alpha Z(m'_\mu/p_\nu)j_{w\mp1}(qr_s)\Big]\mathcal{Y}^{M_f-M_i}_{0wu}(\hat{r}_s)\delta_{wu}$
$\mathcal{M}[1wu\pm]$	$\Big[j_w(qr_s)\pm\alpha Z(m'_\mu/p_\nu)j_{w\mp1}(qr_s)\Big]\mathcal{Y}^{M_f-M_i}_{1wu}(\hat{r}_s,\sigma_s)$
$\mathcal{M}[0wup]$	$ij_w(qr_s)\mathcal{Y}^{M_f-M_i}_{0wu}\sigma_s\cdot\mathbf{p}_s\delta_{wu}$
$\mathcal{M}[1wup]$	$ij_w(qr_s)\mathcal{Y}^{M_f-M_i}_{1wu}(\hat{r}_s,\mathbf{p}_s)$

The large momentum exchange in the muon-capture process, as compared to the beta-decay or electron capture, emphasizes the role of the radial part of the nuclear wave function. As seen in Table 1, the muon-capture matrix elements contain the spherical Bessel function $j_w(qr)$, emerging from the Fourier-Bessel expansion of the final-state lepton wave function. The strong oscillations of the Bessel function interfere with the radial part of the mean-field single-particle wave function. Therefore, the shape of the mean-field potential may have a significant impact on the calculated single-particle transition matrix elements. Typically the muon capture matrix elements have been calculated in the harmonic-oscillator single-particle basis. However, the realistic single-particle potential resembles more the Woods-Saxon potential than the harmonic-oscillator potential. The Woods-Saxon potential can produce noticeable effects on the calculated half-life when compared to the one calculated by using the harmonic-oscillator basis [I].

3.2 Two-neutrino double beta decay

The two-neutrino double beta decay proceeds as virtual transitions via the 1^+ states of the intermediate nucleus. The expression for the inverse half-life in the case of a transition to the ground state of the final nucleus can be factorized as

$$[t^{(2\nu)}_{1/2}(0^+_i \to 0^+_f)]^{-1} = G^{(2\nu)}_{\rm DGT} \ \mid M^{(2\nu)}_{\rm DGT} \mid^2 \ , \tag{27}$$

where $G^{(2\nu)}_{\rm DGT}$ is an integral over the phase space of the leptonic variables [7, 37]. The nuclear matrix element $M^{(2\nu)}_{\rm DGT}$, corresponding to the $2\nu\beta\beta$ decay, can be written as

$$M^{(2\nu)}_{\rm DGT} = \sum_n \frac{(0^+_f \,||\, \sum_j \sigma(j) t^{\mp}_j \,||\, 1^+_n)(1^+_n \,||\, \sum_j \sigma(j) t^{\mp}_j \,||\, 0^+_i)}{(\frac{1}{2}Q_{\beta\beta} + E_n - M_i)/m_{\rm e} + 1} \quad , \tag{28}$$

where the transition operators are the usual Gamow-Teller type of operators for the $\beta^{\mp}$ transitions, $Q_{\beta\beta}$ is the $2\nu\beta\beta$-decay Q value, E_n is the energy of the nth intermediate state, M_i is the mass energy of the initial nucleus, and $m_{\rm e}$ is the rest-mass energy of the electron. Contributions from the Fermi transitions can be neglected [7]. The expression for the half-life in the case of transitions to the exited states of the final nucleus is more complex and can be found in [7].

One could also consider contributions coming from the first-forbidden transitions to the $2\nu\beta\beta$ decay rate. These transitions proceed via the 0^-, 1^- and 2^- states of the intermediate nuclei. In Ref. [38] the authors found notable contributions to the nuclear matrix elements from the 0^- and 1^- channels. However, it has been shown that due to the suppression of the associated phase-space integrals these channels can be neglected [39]. In typical cases this suppression is of the order of 10^{-6} for the first-forbidden channel and stronger for the higher forbidden channels. It has to be mentioned that in the case of the neutrinoless double beta decay the intermediate states other than 1^+ have a non-negligible contribution to the total half-life.

3.3 Neutrinoless double-beta-decay

The most general effective weak-interaction Hamiltonian density, relevant for charged weak currents, can be written as [7, 37]

$$h_{\rm W} = \frac{G_{\rm F}\cos\theta_{\rm C}}{\sqrt{2}} \left(j_{{\rm L}\mu} J^{\mu\dagger}_{\rm L} + \kappa j_{{\rm L}\mu} J^{\mu\dagger}_{\rm R} + \eta j_{{\rm R}\mu} J^{\mu\dagger}_{\rm L} + \lambda j_{{\rm R}\mu} J^{\mu\dagger}_{\rm R} \right) + {\rm h.c.}, \tag{29}$$

where $G_{\rm F}$ is the Fermi coupling constant and $\theta_{\rm C}$ is the mixing angle of the Cabibbo-Kobayashi-Maskawa mechanism for mixing quark flavours. The left- and right-handed leptonic currents are given as follows

$$j_{{\rm L}\mu} = \bar{e}\gamma_\mu (1-\gamma_5)\, \nu_{\rm e,L}\,, \tag{30}$$

$$j_{{\rm R}\mu} = \bar{e}\gamma_\mu (1+\gamma_5)\, \nu'_{\rm e,R}\,, \tag{31}$$

where the weak eigenstates of the neutrino are given in terms of the neutrino mass eigenstates $N_{j{\rm L/R}}$ as

$$\nu_{\rm e,L} = \sum_{j=1}^{2N_{\rm g}} U_{{\rm e}j} N_{j{\rm L}}\,, \tag{32}$$

$$\nu'_{\rm e,R} = \sum_{j=1}^{2N_{\rm g}} V_{{\rm e}j} N_{j{\rm R}}\,, \tag{33}$$

where $N_{\rm g}$ is the number of the neutrino generations. The U and V matrices are the mixing matrices between the weak eigenstates and mass eigenstates of the neutrino. The summations in Eqs. (32) and (33) run to $2N_{\rm g}$ due to the fact that the Majorana-neutrino field $N_{\rm L/R}$ contains the left- and right-handed neutrino fields. The hadronic current of Eq. (29) can be written at quark level as

$$J^{\mu\dagger}_{\rm L/R} = \bar{\rm u}\gamma^{\mu}\left(1 \mp \gamma_5\right){\rm d}\,. \tag{34}$$

By assuming the neutrino mass mechanism to be the dominant one in the $0\nu\beta\beta$ decay (i.e. the right-handed currents are neglected) one can write as a good approximation the inverse of the half-life as

$$\left[t^{(0\nu)}_{1/2}\right]^{-1} = G^{(0\nu)}_1\left(\frac{\langle m_\nu\rangle}{m_{\rm e}}\right)^2\left(M^{(0\nu)}_{\rm GT} - \left(\frac{g_{\rm V}}{g_{\rm A}}\right)^2 M^{(0\nu)}_{\rm F}\right)^2\,, \tag{35}$$

where $m_{\rm e}$ is the mass of the electron and

$$\langle m_\nu\rangle = \sum_j \lambda^{\rm CP}_j m_j |U_{{\rm e}j}|^2 \tag{36}$$

is the effective mass of the neutrino, $\lambda^{\rm CP}_j$ being the CP phase. Furthermore, the quantity $G^{(0\nu)}_1$ of Eq. (35) is the leptonic phase-space factor defined in [7]. The double Gamow-Teller and double Fermi nuclear matrix-elements, which appear in the expression of the $0\nu\beta\beta$ half-life, are defined as follows:

$$M^{(0\nu)}_{\rm F} = \sum_a (0^+_f||h_+(r_{mn},E_a)||0^+_i)\,, \tag{37}$$

$$M^{(0\nu)}_{\rm GT} = \sum_a (0^+_f||h_+(r_{mn},E_a)\sigma_m\cdot\sigma_n||0^+_i)\,. \tag{38}$$

Here summation over a runs over all the intermediate states. The definition of the neutrino potential $h_+(r_{mn},E_a)$ can be found in Refs. [7, 37].

3.4 The OMC as a probe of double beta decay

As mentioned, the OMC can be used to probe the structure of the states of the intermediate nucleus involved in the double-beta-decay transition. The used two-body interaction, in particular the value of the parameter $g_{\rm pp}$ in the case of the pnQRPA, strongly affects the wave functions of the intermediate nucleus. This, in turn, reflects on the one-body transition densities from the initial and final states to the intermediate states of double beta decay. These transition densities are also present in the calculation of the OMC rates to the intermediate states. Thus, by comparing the calculated OMC rates to the experimental ones, one can estimate the reliability of the nuclear matrix elements involved in the double beta decay. It is

worth pointing out that there exists a rather direct bridge between the $2\nu\beta\beta$ decay and the OMC. At the limit $q, Z \to 0$ for the OMC matrix element it follows that

$$\mathcal{M}[101] \to J_{\rm f}^{-1} \frac{\sqrt{3}}{4\pi} M_{\rm GT}\,, \tag{39}$$

where $M_{\rm GT}$ is the reduced Gamow-Teller matrix element appearing in the double-beta-decay nuclear matrix element $M_{\rm DGT}^{(2\nu)}$ of Eq. (28). For the $0\nu\beta\beta$ decay the situation is more complicated. The calculation of the matrix elements $M_{\rm F}^{(0\nu)}$ and $M_{\rm GT}^{(0\nu)}$ involves one-body transition densities for all multipoles in both virtual legs.

There are, however, some drawbacks in the use of the OMC to probe the structure of the states of the $\beta\beta$-decay intermediate nucleus. Firstly, the OMC probes only one of the two legs of a double-beta-decay transition. Secondly, due to the important role of the induced hadronic currents in the OMC, extraction of the relevant information about the matrix elements from the experimental results is more complicated. Lastly, in the nuclear medium the value of the pseudoscalar coupling constant may need to be renormalised from the value given by the PCAC hypothesis. Nevertheless, the OMC offers a versatile tool to study the structure of the intermediate nucleus. In contrast to the beta-decay data, the OMC can be used to study also the exited states of the intermediate nucleus. Moreover, the forbidden transitions in the OMC are not as suppressed as in the case of the beta decay. This allows to study also the intermediate states which are relevant for the $0\nu\beta\beta$ decay.

4 Calculations

4.1 Nuclear-structure calculations

In the case of the light nuclei, the studied double-beta-decaying isobars were $A = 36, 46, 48, 50$. The structure of these nuclei was calculated by using the shell-model code OXBASH. The used interactions in the case of the *sd*-shell $A = 36$ isobars were the USD [1] and SDPOTA [40]. For the *fp*-shell isobars $A = 46$, $A = 48$ and $A = 50$ the interactions used were the FPBP [41] and FPMCC [42]. The structure of the $A = 46$ isobars was calculated in the full fp model space, with no restrictions in the number of configurations. Also for the $A = 48$ isobars the $2\nu\beta\beta$ rate calculations were done in the full *fp*-space. In the case of the $A = 50$ nuclei the JT-dimensions had to be reduced heavily due to computational limits. The truncation was done by requiring the minimum particle occupancy in the $f_{7/2}$ orbital to be 8.

The structure for the medium-heavy nuclei was calculated by using the pnQRPA theory. In the numerical computations the proton model space was taken to be 1p-0f-2s-1d-0g-0h$_{11/2}$. On the neutron side the used model space for ^{76}Se was the same as on the proton side, and in the case of ^{106}Cd the used model space for neutrons was taken to consist of the 1p-0f-2s-1d-0g-2p-1f-0h shells. The corresponding single-particle energies were obtained from the Woods-Saxon well with its parametrization taken from Ref. [43].

The nuclear Hamiltonian for the pnQRPA calculations was obtained from the Bonn one-boson-exchange potential [2], complemented with an empirical renormalization based on phenomenological pairing gaps, the giant Gamow-Teller resonance and spectroscopic data on nuclei close to the relevant isobars. The proton-neutron particle-particle interaction strength was scaled by the parameter $g_{\rm pp}$ which can be used as a free parameter.

4.2 Results for light nuclei

To begin with, the calculated partial OMC rates to the 1^+ states of the final nucleus, as functions of the excitation energy of the final state, are presented in Fig 3. These results are calculated in the harmonic-oscillators single-particle basis. The value for the axial-vector coupling constant was taken to be $g_{\rm A} = -1$ in all our calculations. Furthermore, the ratio $g_{\rm P}/g_{\rm A} = 7$ was used for the pseudo-scalar coupling constant. As can be seen, the strongest transition rates can be found among the few lowest 1^+ states for the case of ^{36}Ar, ^{46}Ti, and ^{48}Ti. However, in the case of ^{50}Cr, the transition rates are more diffused to the higher exited states.

The calculated OMC results can be compared with the ones calculated in the Woods-Saxon single-particle basis. The parametrization for the Woods-Saxon single-particle potential was taken from [43]. In Table 2 the calculated OMC transition rates to the 1^+ states of ^{46}Sc and ^{48}Sc are listed for both the harmonic-oscillator and

Woods-Saxon cases. As can be seen, the transition rates for the different bases are not far from each other, except for some scattered cases.

In Table 3 the calculated $2\nu\beta\beta$ rates for ^{36}Ar, ^{46}Ca, ^{48}Ca, and ^{50}Cr are listed. In these calculations the value $g_{\rm A} = -1.0$ for the axial-vector coupling constant has been adopted. In the case of the $2\nu\beta\beta$ decay of ^{48}Ca the calculated result can be compared with the available experimental one. The experimental result for the $2\nu\beta\beta$ decay of ^{48}Ca is $t_{1/2}^{(2\nu)}(0_i^+ \to 0_f^+) = 4.2^{+3.3}_{-1.3} \times 10^{19}$ y [44]. By evaluating the phase-space integral $G_{\rm DGT}^{(2\nu)}$, the experimental value for the $2\nu\beta\beta$ nuclear matrix element can be obtained. Using $g_{\rm A} = -1.0$, one then obtains $M_{\rm DGT}^{(2\nu)}({\rm exp}) = 0.038^{+0.008}_{-0.009}$. In the case of the $2\nu\beta\beta$ decay of ^{50}Cr there exist an experimental limit $t_{1/2} > 1.3 \times 10^{18}$ y for the half-life of the β^+EC mode [45].

By comparing the experimental value of the $2\nu\beta\beta$-decay matrix element of ^{48}Ca to the calculated one, it can be seen that the used interaction tends to overestimate the value of the matrix element. The corresponding cumulative sum of the $2\nu\beta\beta$-decay matrix element, plotted in Fig. 4, indicates that a few lowest intermediate states give the biggest contribution to the total matrix element. This is partly explained by the energy denominator suppressing the contribution of the higher-lying states. Another reason is that the absolute value of the product of the two GT matrix elements in Eq. (28) is much bigger for these low-lying states than for the other, higher-lying

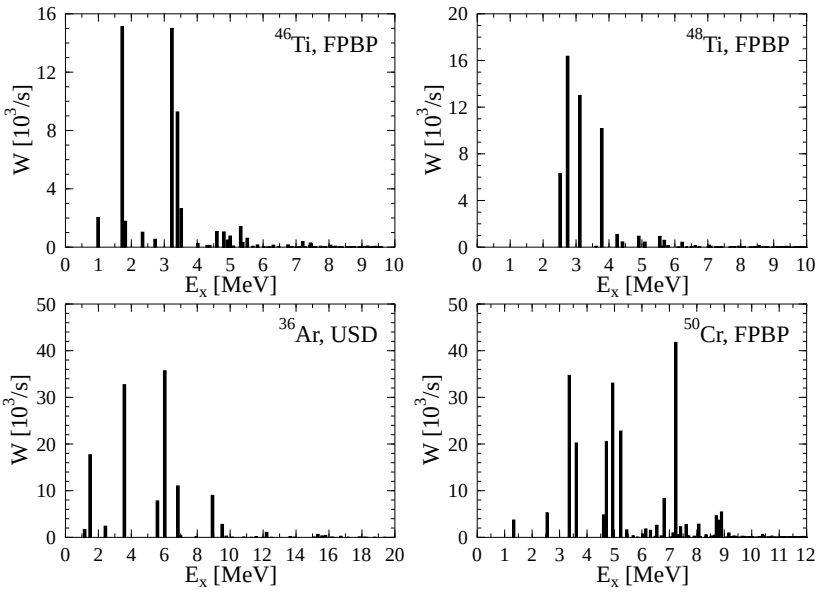

Figure 3: Calculated OMC rates to the 1^+ states of the final nucleus as a function of the excitation energy for four different initial nuclei. The initial nucleus and the used interaction are indicated in each panel. The ratio $g_{\rm P}/g_{\rm A} = 7$ was adopted in the calculations.

Table 2: Calculated partial OMC transition rates for the Woods-Saxon (WS) and harmonic-oscillator (h.o.) single-particle bases using the FPBP interaction. The ratio $g_{\rm P}/g_{\rm A} = 7$ with $g_{\rm A} = -1.0$ has been adopted.

		W [10^3 1/s]				W [10^3 1/s]	
Parent	$J^\pi_{\rm f}$	h.o.	WS	Parent	$J^\pi_{\rm f}$	h.o.	WS
^{46}Ti	1^+_1	2.032	3.433	^{48}Ti	1^+_1	6.310	6.261
	1^+_2	15.123	12.538		1^+_2	16.366	12.029
	1^+_3	1.780	1.754		1^+_3	13.000	11.158
	1^+_4	1.028	0.441		1^+_4	0.080	0.074

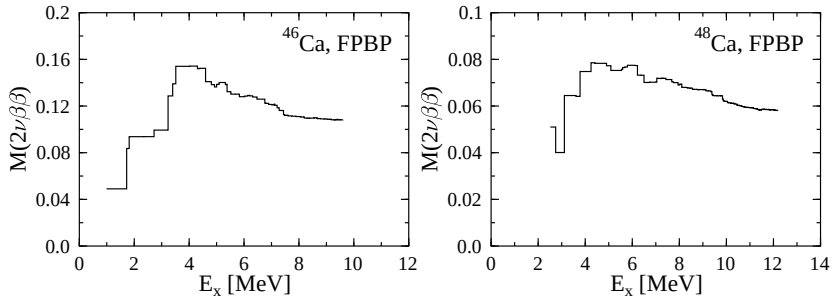

Figure 4: Calculated cumulative sum of the matrix element $M^{(2\nu)}_{\rm DGT}$ of Eq. (28) as a function of the excitation energy of the intermediate state. The $2\nu\beta\beta$ decaying nucleus and the used interaction are indicated in each panel.

Table 3: Calculated DGT matrix elements, Q-values in units of the electron mass ($T = Q/m_{\rm e}$), phase-space factors in units of inverse years, and the corresponding half-lives in units of year for the considered double-beta transitions. The renormalized value $g_A = -1.0$ has been used in all cases.

	^{46}Ca FPBP	^{48}Ca FPBP		^{36}Ar USD (bare)	^{50}Cr FPBP
$T(\beta^-\beta^-)$	1.94	8.36	T(ECEC)	0.84	2.27
$G^{2\nu}_{\rm DGT}$	4.8×10^{-23}	1.6×10^{-17}	$G^{2\nu}_{\rm DGT}$	5.1×10^{-28}	4.9×10^{-25}
$M^{2\nu}_{\rm DGT}$	0.108	0.058	$M^{2\nu}_{\rm DGT}$	0.117	0.097
$t_{1/2}$	1.7×10^{24}	1.8×10^{19}	$t_{1/2}$	1.4×10^{29}	2.1×10^{26}

states. The same reasoning applies also to ^{46}Ca, depicted in the left panel of Fig. 4. Comparison of Figs. 3 and 4 shows that the same intermediate states are relevant

for the OMC and $2\nu\beta\beta$ decay. Therefore, measurements of the partial OMC rates to these low-lying states of the intermediate nucleus could give some valuable information about the involved nuclear structure. This information is also useful in the case of the $0\nu\beta\beta$-decay rate calculations.

4.3 Medium heavy nuclei

In the case of the medium heavy nuclei the OMC rates were calculated for the nuclei ^{76}Se, ^{82}Kr, ^{100}Ru, ^{106}Cd, ^{110}Cd, ^{116}Sn, ^{128}Xe, and ^{136}Ce. The OMC on these nuclei leads to the odd-odd nuclei ^{76}As, ^{82}Br, ^{100}Tc, ^{106}Ag, ^{110}Ag, ^{116}In, ^{128}I, and ^{136}La, which are involved as providing intermediate states in the double beta decays of the nuclei ^{76}Ge, ^{82}Se, ^{100}Mo, ^{106}Cd, ^{110}Pd, ^{116}Cd, ^{128}Te, and ^{136}Ce. Two of the decays, namely ^{106}Cd $\rightarrow$ ^{106}Ag and ^{136}Ce $\rightarrow$ ^{136}Ba, are $\beta^+\beta^+$ type of transitions, while the rest are $\beta^-\beta^-$ type of transitions. All of the chosen isobaric triplets contain low-lying 1^+ or 2^- states in the involved intermediate double-odd nucleus.

Table 4: Total muon-capture rates to the 1^+ or 2^- states (column 6) in the transitions of column 5. The ratio $g_{\rm P}/g_{\rm A} = 7$ was used. The $g_{\rm pp}$ value of column 3 is chosen such that the experimental $\log ft$ value [46] (column 2) can be roughly reproduced (column 4) in a specific beta-decay transition (column 1).

Beta decay	$\log ft$ (exp)	$g_{\rm pp}$	$\log ft$ (th.)	Muon capture	$W_{\rm tot}$ [10^3 1/s]
^{76}As$(1^+_1) \rightarrow$ ^{76}Se$(0^+_{\rm g.s.})$	-	0.9	5.8	^{76}Se $\rightarrow$ ^{76}As(1^+)	114
^{76}As$(2^-_{\rm g.s.}) \rightarrow$ ^{76}Se$(0^+_{\rm g.s.})$	9.7	1.0	8.7	^{76}Se $\rightarrow$ ^{76}As(2^-)	1529
^{82}Br$(2^-_1) \rightarrow$ ^{82}Kr$(0^+_{\rm g.s.})$	8.9	1.0	8.9	^{82}Kr $\rightarrow$ ^{82}Br(2^-)	1497
^{100}Tc$(1^+_{\rm g.s.}) \rightarrow$ ^{100}Ru$(0^+_{\rm g.s.})$	4.6	1.1	4.4	^{100}Ru $\rightarrow$ ^{100}Tc(1^+)	3734
^{100}Tc$(2^-_1) \rightarrow$ ^{100}Ru$(0^+_{\rm g.s.})$	-	1.0	8.9	^{100}Ru $\rightarrow$ ^{100}Tc(2^-)	1889
^{106}Ag$(1^+_{\rm g.s.}) \rightarrow$ ^{106}Cd$(0^+_{\rm g.s.})$	> 4.2	0.8	4.3	^{106}Cd $\rightarrow$ ^{106}Ag(1^+)	4635
^{110}Ag$(1^+_{\rm g.s.}) \rightarrow$ ^{110}Cd$(0^+_{\rm g.s.})$	4.7	0.9	4.7	^{110}Cd $\rightarrow$ ^{110}Ag(1^+)	4650
^{110}Ag$(2^-_1) \rightarrow$ ^{110}Cd$(0^+_{\rm g.s.})$	-	1.0	9.2	^{110}Cd $\rightarrow$ ^{110}Ag(2^-)	1635
^{116}In$(1^+_{\rm g.s.}) \rightarrow$ ^{116}Sn$(0^+_{\rm g.s.})$	4.7	1.0	4.7	^{116}Sn $\rightarrow$ ^{116}In(1^+)	5102
^{116}In$(2^-_1) \rightarrow$ ^{116}Sn$(0^+_{\rm g.s.})$	-	1.0	13.1	^{116}Sn $\rightarrow$ ^{116}In(2^-)	1430
^{128}I$(1^+_{\rm g.s.}) \rightarrow$ ^{128}Xe$(0^+_{\rm g.s.})$	6.1	1.0	6.3	^{128}Xe $\rightarrow$ ^{128}I(1^+)	5835
^{128}I$(2^-_1) \rightarrow$ ^{128}Xe$(0^+_{\rm g.s.})$	-	1.0	9.4	^{128}Xe $\rightarrow$ ^{128}I(2^-)	1270
^{136}La$(1^+_{\rm g.s.}) \rightarrow$ ^{136}Ce$(0^+_{\rm g.s.})$	-	1.0	8.2	^{136}Ce $\rightarrow$ ^{136}La(1^+)	4423
^{136}La$(2^-_1) \rightarrow$ ^{136}Ce$(0^+_{\rm g.s.})$	-	1.0	9.7	^{136}Ce $\rightarrow$ ^{136}La(2^-)	1383

In Table 4 the calculated results for the total OMC rates to the 1^+ and 2^- final states are presented. In these calculations the ratio $g_{\rm P}/g_{\rm A} = 7$ was used. The value of the parameter $g_{\rm pp}$ has been chosen such that the corresponding experimental $\log ft$

value can be roughly reproduced. As mentioned, the $g_{\rm pp}$ strongly affects the calculated nuclear structure, in particular the wave function of the lowest 1^+ state. This can be seen in Fig. 5, where the partial OMC rates to the 1^+_1 states of several final nuclei have been plotted as functions of $g_{\rm pp}$. The same shown $g_{\rm pp}$ dependance can be found in the $2\nu\beta\beta$ decay rates, and in fact the measured $2\nu\beta\beta$ half-lives can be reproduced by suitably choosing the value of $g_{\rm pp}$ [47]

Fig. 5 also illustrates the break-down of the pnQRPA theory at large values of the $g_{\rm pp}$ parameter. Due to the excessive growth of correlations in the pnQRPA ground-state, the calculations produce unphysically large values for the capture rates. This break-down of the pnQRPA theory can also be seen in the $\beta\beta$ matrix elements at large values of $g_{\rm pp}$ [47].

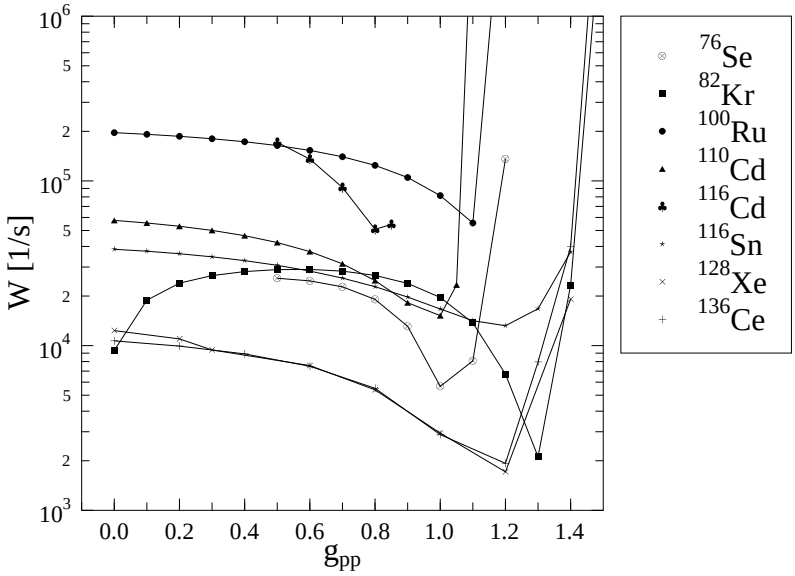

Figure 5: Calculated OMC rates from the ground state of the indicated nuclei to the 1^+_1 states of the final nucleus as functions of the particle-particle interaction strength parameter $g_{\rm pp}$. The ratio $g_{\rm P}/g_{\rm A} = 7$ has been used.

In addition to the parameter $g_{\rm pp}$, there is also another parameter present in the capture rate calculations with somewhat uncertain value, namely the pseudoscalar coupling constant $g_{\rm P}$. The capture rate W has a parabolic behavior as a function of the $g_{\rm P}$. Thus, when a experimental measurement of the partial capture rate is made, it translates to a certain area in the $g_{\rm P}$ and $g_{\rm pp}$ parameter spaces. By measuring partial capture rates to few lowest states, the intersection of the corresponding parameter spaces should hopefully become small enough to yield a rather restricted value for these parameters.

5 Discussion and conclusions

The main focus of the present work is in the nuclear-structure aspects of the OMC process. Publication [I] discusses the effect of the mean-field parameters on the OMC observables. The Publications [II-VI] concentrate on the use of the OMC as a probe of virtual transitions of double beta decays. Due to the fact that the structure of the intermediate states of double beta decay has a strong impact on the calculated values of the matrix elements, for both $2\nu\beta\beta$ and $0\nu\beta\beta$ decays, one needs a method to evaluate the reliability of the used nuclear model. Publications [II-VI] demonstrate how to use the OMC to probe one branch of the $\beta\beta$ transition. The nuclear models employed in the OMC rate calculations of the present work are the nuclear shell-model and the pnQRPA. These two models are also the ones most used in $\beta\beta$ calculations.

In Publication [I] the effect of the nuclear mean field on the muon capture observables was studied. Due to the interference of the oscillating Bessel function $j_w(qr)$ and the single-particle wave function the shape of the mean field potential has an impact on the calculated OMC matrix elements. The calculated results of the OMC rates in the harmonic-oscillator and Woods-Saxon single-particle bases did show some differences. However, differences were usually small and never significant. The same was also pointed out in Publication [VI] in the case of the OMC of ^{46}Ti and ^{48}Ti. Also, the results for the angular correlation parameter x in [I] were found to be quite similar in both single-particle bases.

Although the calculated values of the OMC rates depend on the used interaction, it was found in [V] that in the case of the $A = 36$ isobars it there were no large differences between the USD and SDPOTA interactions in the total capture rates to 1^+ states. This happened even though the transition rates to the individual states differed. The same kind of phenomenon was also noted in the $2\nu\beta\beta$-decay matrix element of ^{36}Ar. The value of the total matrix element $M^{(2\nu)}_{\rm DGT}$ was quite similar in both cases, although there were some differences in the shape of the cumulative sum.

In the calculations of the fp-shell nuclei it was found that in the OMC of ^{46}Ti and ^{48}Ti the biggest transition rates were among the transitions to the few lowest 1^+ final states. These states were also important in the $2\nu\beta\beta$ decay. The OMC rate calculations of Publication [V] indeed indicate some differences between the FPBP and FPMCC interactions. The OMC rates for ^{46}Ti and ^{48}Ti were also calculated in [V] with different values of the pseudoscalar coupling constant $g_{\rm P}$. These calculations indicate surprisingly small dependence on $g_{\rm P}$ in many cases. This helps the nuclear-structure analysis, when the calculated partial OMC rates are compared to the experimental ones. The first experiments on the OMC of ^{48}Ti have been performed at the PSI [48]. Concerning the OMC of ^{50}Cr it was found that the captures favour more the higher energy 1^+ final states than in the other calculated cases. It was also noted that the partial OMC rates did not wary much as functions of $g_{\rm P}$.

A number of $2\nu\beta\beta$ rates were calculated in [V]. In addition to the results quoted in the previous section, the shape of the calculated cumulative sum of the matrix

element $M^{(2\nu)}_{\rm DGT}$ was studied also for ^{48}Ca. It was found that the strong transitions through few low-lying 1^+ states were mainly transition involving the $0f_{7/2}$ orbital. Contributions of transitions through the higher-lying 1^+ states typically decreased the value of the total matrix element. The involved single-particle transitions were mainly $0f_{7/2} \rightarrow 0f_{5/2} \rightarrow 0f_{7/2}$. This same behaviour was seen for both the FPBP and FPMCC interactions. In Publication [IV] it was noted that FPBP and FPMCC interactions produce quite similar values for the total $2\nu\beta\beta$ decay matrix element. However, the shape of the cumulative sum had differences. Nevertheless, the common feature for all the calculated cases of $2\nu\beta\beta$ decay of ^{46}Ca and ^{48}Ca was that the transitions through a few lowest 1^+ states dominated the total matrix element. This was also displayed in Publications [IV, V] in the plot of the product of the two Gamow-Teller matrix elements of Eq. (28) as a function of the excitation energy of the intermediate state. For ^{50}Cr it was pointed out in [V] that the experimental limit of [45] was far from the calculated value of the half-life.

In the case of the heavier nuclei the individual OMC rates had a strong dependence on the particle-particle interaction strength parameter $g_{\rm pp}$, as can be seen in Publication [III]. However, the strong dependence on $g_{\rm pp}$ tends to vanish when the partial capture rates are summed up to the total capture rates to the 1^+ or 2^- states. In [III] the involved matrix elements of the OMC were analyzed. It was found that the matrix element $\mathcal{M}[101]$, involved in transitions to the 1^+ states, is typically more sensitive to $g_{\rm pp}$ than the matrix element $\mathcal{M}[112]$, which appear in transitions to the 2^- states. This also reflects in the partial capture rates. The break-down of the pnQRPA at large values of $g_{\rm pp}$ was also seen in some matrix elements. It was found that the partial and total OMC rates clearly depend on the pseudoscalar coupling constant $g_{\rm P}$. Thus, there are actually two relevant parameters in the calculations. The $\log ft$ values of β decays of the intermediate nuclei to the ground states of the final or initial nuclei of double beta decay were discussed in [III]. In many cases the experimental $\log ft$ value was unknown.

In conclusion, the formalism of the OMC has been presented and its connection to the double beta decay explored. It has been shown that the partial OMC rates can be used to probe the intermediate states of double beta decay. Furthermore, results on the partial OMC rates have been presented for several nuclei. The nuclear structure for the light nuclei was handled with the nuclear shell model. In the case of the heavier nuclei the pnQRPA was used for the nuclear-structure calculations. For the lighter nuclei it was found that 1^+ states with large OMC transition rate were also the ones which gave the dominant contributions for the $2\nu\beta\beta$ decay. The effect of the mean field on the OMC rates was also discussed. For ^{48}Ca the calculated $2\nu\beta\beta$-decay rates were compared to the experiment. In the case of the heavier nuclei, strong dependence of the OMC rates on the particle-particle interaction strength parameter $g_{\rm pp}$ was found. Also, the role of the pseudoscalar coupling constant $g_{\rm P}$ was discussed.

References

[I] Publication I of this thesis.

[II] Publication II of this thesis.

[III] Publication III of this thesis.

[IV] Publication IV of this thesis.

[V] Publication V of this thesis.

[VI] Publication VI of this thesis.

[1] B.H. Wildenthal, Prog. Part. Nucl. Phys. **11** (1984) 5.

[2] K. Holinde, Phys. Rep. **68** (1981) 121.

[3] M.G. Mayer, Phys. Rev. **74** (1948) 235;
M. Goeppert Mayer, Phys. Rev. **75** (1949) 1969.

[4] B.A. Brown, A. Etchegoyen and W.D.M. Rae, the computer code OXBASH, MSU-NSCL Report **524** (1988).

[5] J.A. Halbleib and R.A. Sorensen, Nucl. Phys. A **98** (1967) 542.

[6] J. Suhonen, T. Taigel and A. Faessler, Nucl. Phys. A **486** (1988) 91.

[7] J. Suhonen and O. Civitarese, Phys. Rep. **300** (1998) 123.

[8] M. Baranger, Phys. Rev. **120** (1960) 957.

[9] E. Fermi, Z. Physik **88** (1934) 161.

[10] S. Weinberg, Phys. Rev. Lett. **19** (1967) 1264.

[11] The Super-Kamiokande Collaboration, Phys. Rev. Lett. **81** (1998) 1562.

[12] The SNO Collaboration, Phys. Rev. Lett. **89** (2002) 011301.

[13] KamLAND Collaboration, Phys. Rev. Lett. **90** (2003) 021802.

[14] M. Appollonio *et al.*, Phys. Lett. B **466** (1999) 415.

[15] D.N. Spergel *et al.*, Astrophys. J. Suppl. **148** (2003) 175.

[16] Ch. Kraus *et al.*, Eur. Phys. J. C **40** (2005) 447.

[17] M. Goeppert-Mayer, Phys. Rev. **48** (1935) 512.

[18] V. Tretyak and Y. Zdesenko, At. Data Nucl. Data Tables **80** (2002) 83.

[19] W.H. Furry, Phys. Rev. **56** (1939) 1184.

[20] J. Schecher and J.W.F. Valle, Phys. Rev. D **25** (1982) 2951.

[21] O. Civitarese and J. Suhonen, Nucl. Phys. A **729** (2003) 867.

[22] H.V. Klapdor-Kleingrothaus, Nucl. Phys. B (Proc. Suppl.) **143** (2005) 229.

[23] C.E. Aalseth *et. al.*, Mod. Phys. Lett. A **17** (2002) 1475.

[24] Yu.G. Zdesenko, F.A. Danevich and V.I. Tretyak, Phys. Lett. B **546** (2002) 206.

[25] M. Aunola and J. Suhonen, Nucl. Phys. A **602** (1996) 113.

[26] V.A. Rodin, A. Faessler, F. Šimkovic and P. Vogel, Phys. Rev. C **68** (2003) 044302.

[27] J. Suhonen, Nucl. Phys. A **752** (2005) 53.

[28] C. Volpe, J. Phys. G **31** (2005) 903.

[29] O. Civitarese and J. Suhonen, Phys Lett. B **626** (2005) 80.

[30] D.F. Measday, Phys. Rep. **354** (2001) 243.

[31] E. Kolbe, K. Langanke and K. Riisager, Eur. Phys. J. A **11** (2001) 39.

[32] M. Morita and A. Fujii, Phys. Rev. **118** (1960) 606.

[33] J.S. Towner, Phys. Rep. **155** (1987) 263.

[34] B.A. Brown and B.H. Wildenthal, Ann. Rev. Nucl. Part. Sci **38** (1988) 29.

[35] A. de Shalit and I. Feshbach, Theoretical Nuclear Physics vol I, (Wiley & Sons, 1974).

[36] V. Gillet and D.A. Jenkins, Phys. Rev. **140** (1965) B32.

[37] M. Doi, T. Kotani and E. Takasugi, Prog. Theor. Phys. Suppl. **83** (1985) 1.

[38] C. Barbero, F. Krampotić and A. Mariano, Phys. Lett. B **345** (1995) 192.

[39] O. Civitarese and J. Suhonen, Nucl. Phys. A **607** (1996) 152.

[40] B.A. Brown, W.A. Richter, R.E. Julies and B.H. Wildenthal, Ann. Phys. **182** (1988) 191.

[41] W.A. Richter, *et al.*, Nucl. Phys. A **523** (1991) 325.

[42] J.B. McGrory, B.H. Wildenthal and E.C. Halbert, Phys. Rev. C **2** (1970) 186.

[43] A. Bohr and B.R. Mottelson, Nuclear structure, vol. I (Benjamin, New York, 1969).

[44] V.B. Brudanin, *et al.*, Phys. Lett. B **495** (2000) 63.

[45] I. Bikit, *et al.*, Phys. Rev. C **67** (2003) 065801.

[46] R.B. Firestone, V.S. Shirley, S.Y. Chu, C.M. Baglin and J. Zipkin, Table of Isotopes CD-ROM, 8th Ed. Version 1.0 (Wiley-Interscience, New York, 1996).

[47] J. Suhonen, Phys. Lett. B **607** (2005) 87.

[48] Ch. Briancon, *et al.*, The R-97-03 Experiment and Its Extension (μCR42β) at the PSI.